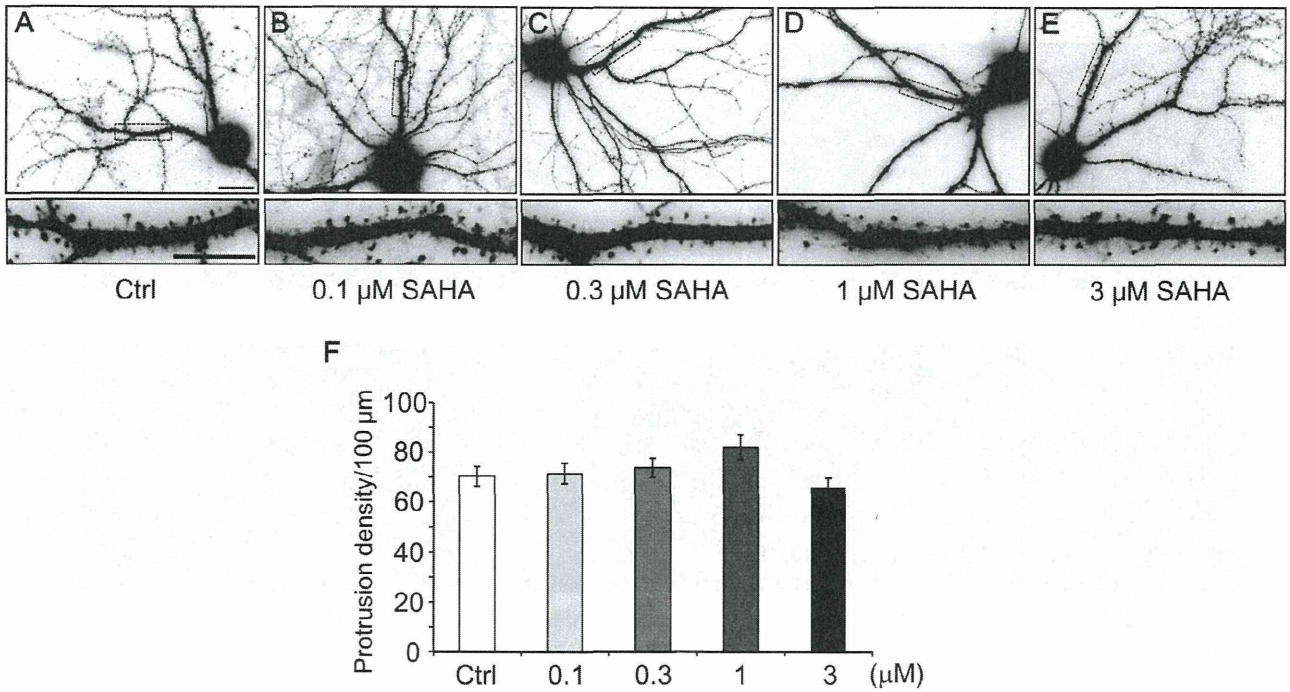

Fig. 3. Acute effect of SAHA on the density of protrusions. GFP-transfected neurons (21 DIV) were treated with various dosages of SAHA (0.1, 0.3, 1, 3 μM) for 24 h. (A–E) GFP-fluorescence images of neurons. Lower images are high magnification images of the area in the rectangle in the upper images. (F) Quantification of the density of protrusions along dendrites. Data are presented as means ± SEM, $n = 26$, 35, 33, 21 and 25 cells for control, 0.1, 0.3, 1 and 3 μM, respectively, $P = 0.177$, ANOVA. Scale bars: low magnification images, 20 μM; high magnification images, 10 μM.

ensure complete re-suspension. The peptide was then diluted with sterile phosphate buffer to 100 μM. This solution was vortexed and incubated at 4 °C for 24 h and then centrifuged to remove insoluble aggregates. The supernatant was used as the source of ADDLs in this study. We analyzed the oligomerization of $A\beta_{1-42}$ and the ADDLs by Western blotting (Fig. 1). The concentration of ADDLs was calculated according to the equivalent amount of $A\beta_{1-42}$ used in preparing the ADDL solution.

2.3. Cell culture and cDNA transfection

All animal experiments were performed according to the guidelines of the Animal Care and Experimentation Committee (Gunma University, Showa Campus, Maebashi, Japan). Every effort was made to minimize animal suffering and to reduce the number of animals used.

Fertilized female C57BL/6NCrSlc mice were purchased from Japan SLC, Inc. (Hamamatsu, Japan). Primary hippocampal cultures were prepared according to previously described methods (Takahashi et al., 2003). Briefly, after deep anesthesia, hippocampal neurons were prepared from embryonic 16-day-old mice and plated on coverslips coated with poly-L-lysine (1 mg/ml) in Minimum Essential Medium (MEM; Life Technologies, Carlsbad, CA, USA) supplemented with 10% fetal bovine serum. After attachment of cells, the coverslips were transferred into a dish containing a glial monolayer sheet and maintained in the serum-free MEM with B-27 supplement (Life Technologies). After the cells were incubated for 21 days *in vitro* (DIV), they were pharmacologically treated, and then analyzed biochemically and immunocytochemically. SAHA, an inhibitor of class I and II HDACs, was dissolved in DMSO, and cultured neurons were treated with either SAHA or vehicle as control (final concentration of DMSO, 0.05%). For protrusion density analysis, cells were transfected with pEGFP-C1 vector (Clontech, Palo Alto, CA, USA) using Lipofectamine 2000 Transfection Reagent (Life Technologies) at 7 DIV.

2.4. Electrophoresis and Western blotting

Sodium dodecyl sulfate–polyacrylamide gel electrophoresis (SDS–PAGE) and Western blotting were performed as described previously (Takahashi et al., 2003; Ishizuka et al., 2013). Briefly, cells from 10 coverslips were harvested in 500 μl Tris-buffered saline (TBS), pH 7.4, containing 20 mM NaF, 1 mM Na_3VO_4 and a protease inhibitor cocktail, Complete Mini (Roche, Indianapolis, IN, USA). After centrifugation, the cell pellet was solubilized in 100 μl cell lysis buffer (10 mM Tris–HCl, 150 mM NaCl, 2% SDS, 20 mM NaF, 1 mM Na_3Vo_4 and the protease inhibitor cocktail) and sonicated. After centrifugation, supernatant was collected and protein concentrations were determined using the DC protein assay kit (Bio-Rad Laboratories, Inc., Hercules, CA, USA).

Equal amounts of protein (10–20 μg/lane) were subjected to SDS–PAGE and transferred to Immobilon-P polyvinylidene difluoride membranes (Merck Millipore). The membranes were incubated with the appropriate primary and secondary antibodies. Peroxidase activity was detected using chemiluminescence reagents (Immobilon Western Chemiluminescent HRP Substrate, Merck Millipore) and visualized with an image analyzer (LAS-3000, Fujifilm, Tokyo, Japan).

2.5. Immunocytochemistry

Cultured neurons were fixed with 4% paraformaldehyde in phosphate buffered saline (PBS), pH 7.4, for 20 min at room temperature. After permeabilization with 0.1% Triton X-100 in PBS, the cells were incubated with 3% bovine serum albumin in PBS for 1 h at room temperature, and then incubated with primary antibodies overnight at 4 °C. After washing with PBS, the cells were incubated with the appropriate secondary antibodies for 1 h at room temperature. Fluorescence images of cells were obtained with an Axio Imager Z2 microscope (Zeiss, Jena, Germany), and captured fluorescence images were analyzed using MetaMorph

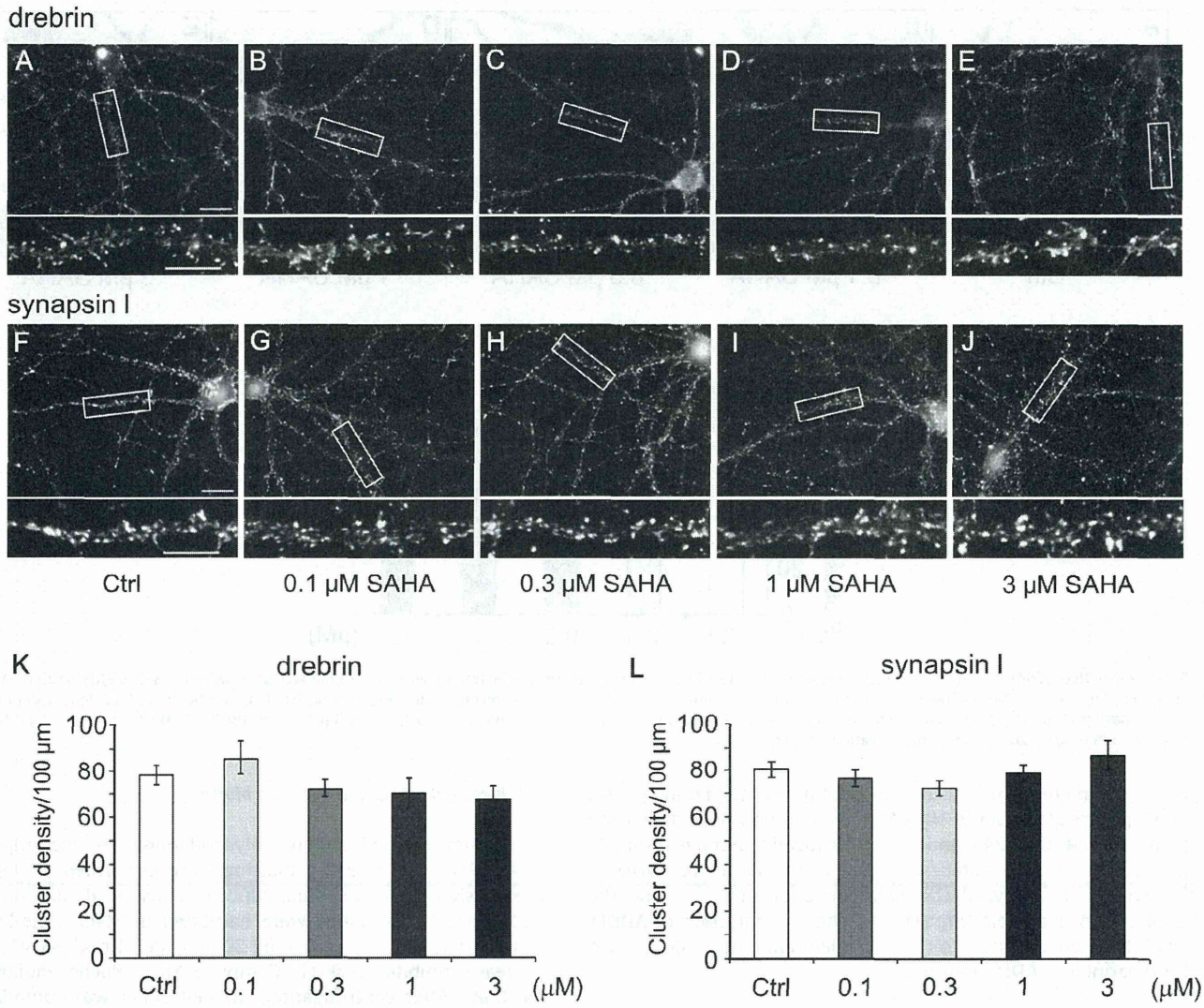

Fig. 4. Acute effect of SAHA on drebrin and synapsin I cluster density. Cultured neurons (21 DIV) were treated with 1 μM SAHA for 24 h. (A–E) Fluorescence images of cultured neurons immunostained with anti-drebrin antibody. (F–J) Fluorescence images of cultured neurons immunostained with anti-synapsin I antibody. Lower images are high magnification images of the area in the rectangle in the upper images. (K and L) Quantification of drebrin and synapsin I cluster density along dendrites. Data are presented as means ± SEM; drebrin, $n = 20$ cells, $P = 0.213$, ANOVA; synapsin I, $n = 50$ cells for control, 0.1, 0.3 and 1 μM, $n = 35$ cells for 3 μM, $P = 0.207$, ANOVA. Scale bars: low magnification images, 20 μM; high magnification images, 10 μm.

software (Molecular Devices, Sunnyvale, CA, USA). Images for presentation were prepared using Adobe Photoshop software (Adobe Systems, San Jose, CA, USA).

2.6. Quantification

Each protein cluster was defined as a round immunofluorescent region with a peak fluorescence intensity twofold greater than the average fluorescence intensity of dendrites, and were counted along the dendrite (Takahashi et al., 2003). Dendritic protrusions >0.5 and <8 μM in length were analyzed in this study. Classification of dendritic protrusions into spines or filopodia was performed as described previously (Yamazaki et al., 2014). Data were statistically analyzed by analysis of variance (ANOVA), and post hoc testing was performed using Dunnett's test (comparison with control group) or Bonferroni's test (comparisons between multiple groups). All data are presented as mean ± standard error of the mean (SEM). A P-value <0.05 was considered significant.

3. Results

3.1. SAHA treatment does not affect dendritic protrusion density

We first examined whether SAHA treatment induces histone acetylation, and whether it affects protrusion density along dendrites. We treated 21-DIV neurons with various dosages of SAHA (0.1, 0.3, 1, 3 μM) for 1 and 24 h. Western blot analyses showed that SAHA treatment significantly increased the acetylation of histone H3 protein at Lys9 and 14 ($n = 3$ experiments, Dunnett's test; Fig. 2). It was reported that chronic SAHA administration for 10 days increases dendritic spine density *in vivo* (Guan et al., 2009). To test the acute effect of SAHA treatment on protrusion density, we treated GFP-transfected neurons (21 DIV) with various dosages of SAHA (0.1, 0.3, 1, 3 μM) for 24 h and measured the density of protrusions. The density of protrusions was not altered by any dosage of SAHA ($n = 26$ cells for control, $n = 35$ for 0.1 μM, $n = 33$ for 0.3 μM, $n = 21$ for 1 μM, $n = 25$ for 3 μM; $P = 0.177$, ANOVA; Fig. 3).

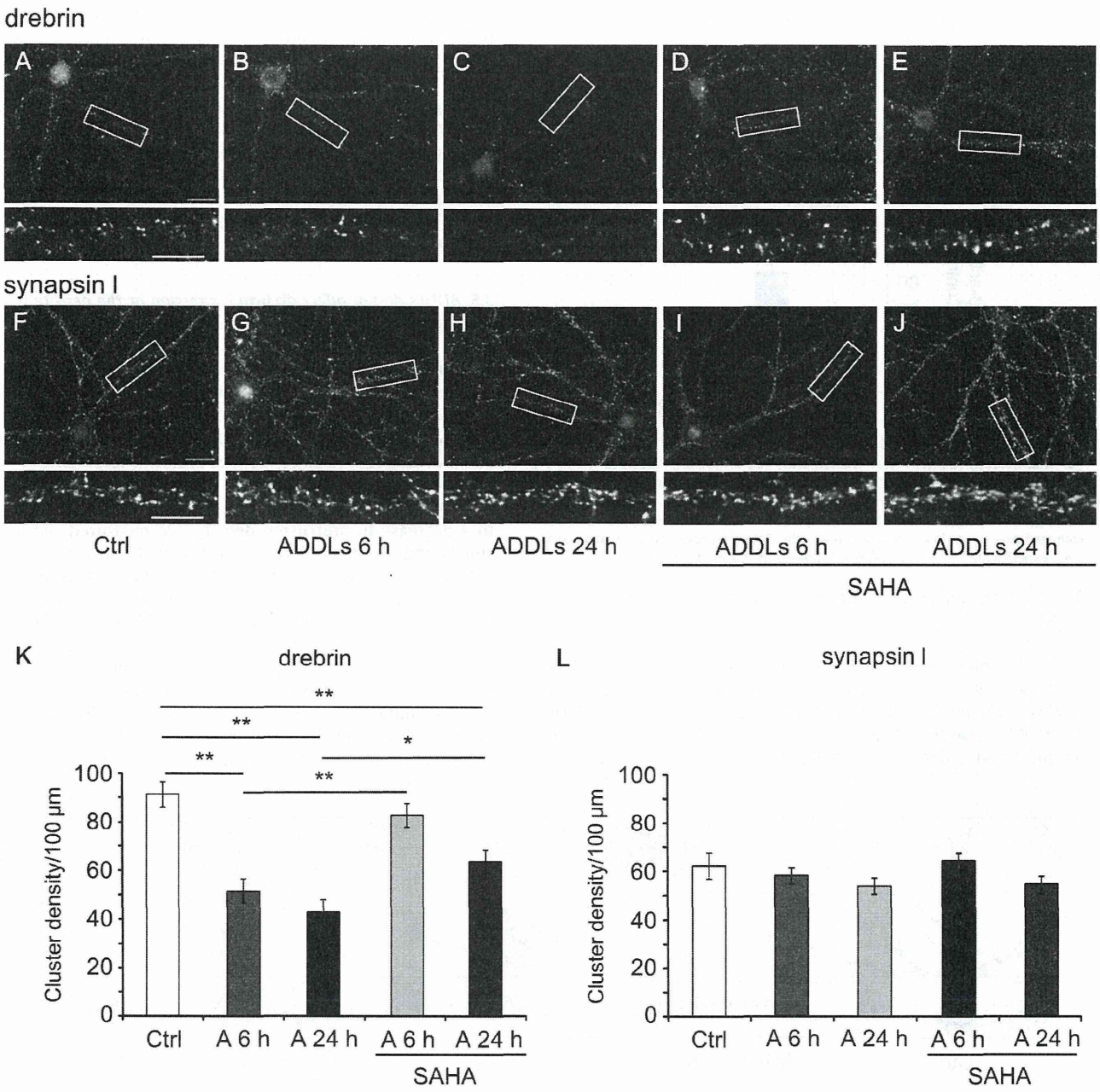

Fig. 5. Effect of SAHA on drebrin and synapsin I cluster density in ADDL-treated neurons. Cultured neurons were treated with 1 μM SAHA for 1 h prior to treatment with 100 nM ADDLs for 6 and 24 h. Immunofluorescence images of drebrin (A–E) and synapsin I (F–J). Lower images are high magnification images of the area in the rectangle in the upper images. Quantification of drebrin (K) and synapsin I (L) cluster density along dendrites. Data are presented as means ± SEM; $n = 35$ cells for control, ADDLs 6 h, ADDLs 24 h, SAHA + ADDLs 24 h; $n = 34$ for SAHA + ADDLs 6 h; $^{*}P < 0.05$, $^{**}P < 0.01$, ANOVA, followed by Bonferroni's post hoc test. A 6 h and A 24 h indicate ADDL treatments of 6 and 24 h, respectively (K and L). Scale bars: low magnification images, 20 μM; high magnification images, 10 μm.

3.2. SAHA treatment does not affect drebrin or synapsin I cluster density along dendrites

We next examined whether SAHA treatment directly affects drebrin and synapsin I cluster density along dendrites. Immunocytochemical analyses showed that neither drebrin nor synapsin I cluster density along dendrites was altered by treatment with any of the different dosages of SAHA for 24 h (drebrin, $n = 20$ cells, $P = 0.213$; synapsin I, $n = 50$ cells for control, 0.1, 0.3 and 1 μM, $n = 35$ cells for 3 μM, $P = 0.207$; ANOVA; Fig. 4).

3.3. ADDLs reduce drebrin cluster density

We treated 21-DIV neurons with 100 nM ADDLs for 6 and 24 h. In ADDL-treated neurons, drebrin and synapsin I clusters were distributed along dendrites similar to that in control neurons (Fig. 5A–J). However, drebrin cluster density in the ADDL-treated neurons was significantly decreased at both 6 and 24 h compared with control neurons ($n = 35$ cells, ANOVA, followed by Bonferroni's post hoc test; Fig. 5K). In comparison, synapsin I cluster density was not altered in ADDL-treated neurons ($n = 30$ cells, $P = 0.223$, ANOVA, Fig. 5L).

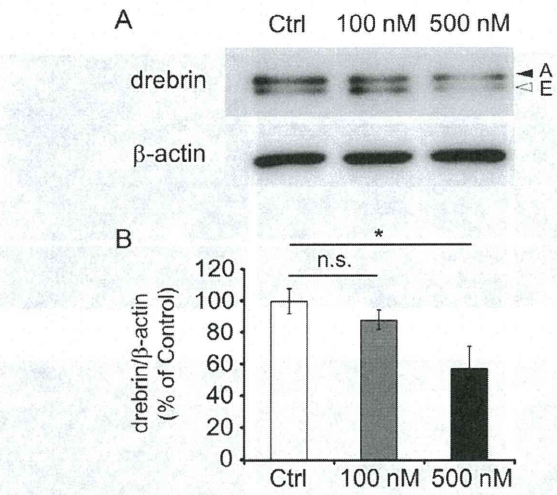

Fig. 6. Effect of ADDLs on drebrin expression, analyzed by Western blotting. Cultured neurons (21 DIV) were treated with 100 or 500 nM ADDLs for 24 h. (A) Upper panel shows a typical Western blot for drebrin. Closed and open arrowheads indicate drebrin A and drebrin E, respectively. Lower panel shows β-actin as a loading control. (B) Western blots were quantified with NIH ImageJ software after standardizing the ratio of drebrin and β-actin. Data are presented as means ± SEM., $n = 3$ experiments; $^*P < 0.05$, ANOVA, followed by Dunnett's post hoc test.

3.4. SAHA attenuates the ADDL-induced decrease in drebrin cluster density

To examine whether SAHA attenuates the ADDL-induced decrease in drebrin cluster density, we added 1 μM SAHA to the culture medium for 1 h prior to treatment with 100 nM ADDLs. After 6 h, drebrin cluster density in ADDL-treated neurons administered SAHA was significantly higher than in those not administered SAHA (Fig. 5B and D), and was similar to that in control neurons (Fig. 5A and D). After 24 h, drebrin cluster density in ADDL-treated neurons administered SAHA was also significantly higher than in those not administered SAHA (Fig. 5C and E), although it was significantly lower than in control neurons (Fig. 5A and E). As expected, neither synapsin I distribution pattern nor cluster density was affected by ADDL or SAHA treatment ($n = 30$ cells for control, $n = 30$ for ADDLs 6 h, $n = 31$ for SAHA 24 h, $n = 30$ for SAHA + ADDLs 6 h, $n = 23$ for SAHA + ADDLs 24 h; $P = 0.223$, ANOVA). These results indicate that SAHA attenuates the toxicity of ADDLs.

3.5. ADDLs do not affect drebrin expression or the density of protrusions

To examine whether the ADDL-induced drebrin loss is due to a decrease in drebrin expression, we analyzed neurons treated with 100 nM and 500 nM ADDLs for 24 h by Western blotting. At 100 nM, ADDLs did not reduce the expression of drebrin, but at 500 nM, they significantly reduced drebrin expression ($n = 3$ experiments, Dunnett's test, Fig. 6).

Next, to examine whether the ADDL-induced drebrin loss is due to a decrease in protrusion density, we measured the density of spines and filopodia along dendrites in GFP-transfected neurons (21 DIV) treated with 100 nM ADDLs for 24 h. The protrusion density was not altered by the ADDL treatment for 24 h ($n = 28$, 28, 29, 27 and 33 cells for control, ADDLs 6 h, ADDLs 24 h, SAHA + ADDLs 6 h and SAHA + ADDLs 24 h, respectively; total protrusion density, $P = 0.295$; spine density, $P = 0.145$; filopodium density, $P = 0.105$, ANOVA; Fig. 7). These results indicate that 100 nM ADDLs alter the distribution of drebrin without reducing drebrin expression or protrusion density, and that HDAC inhibition attenuates ADDL-induced drebrin loss from dendritic spines.

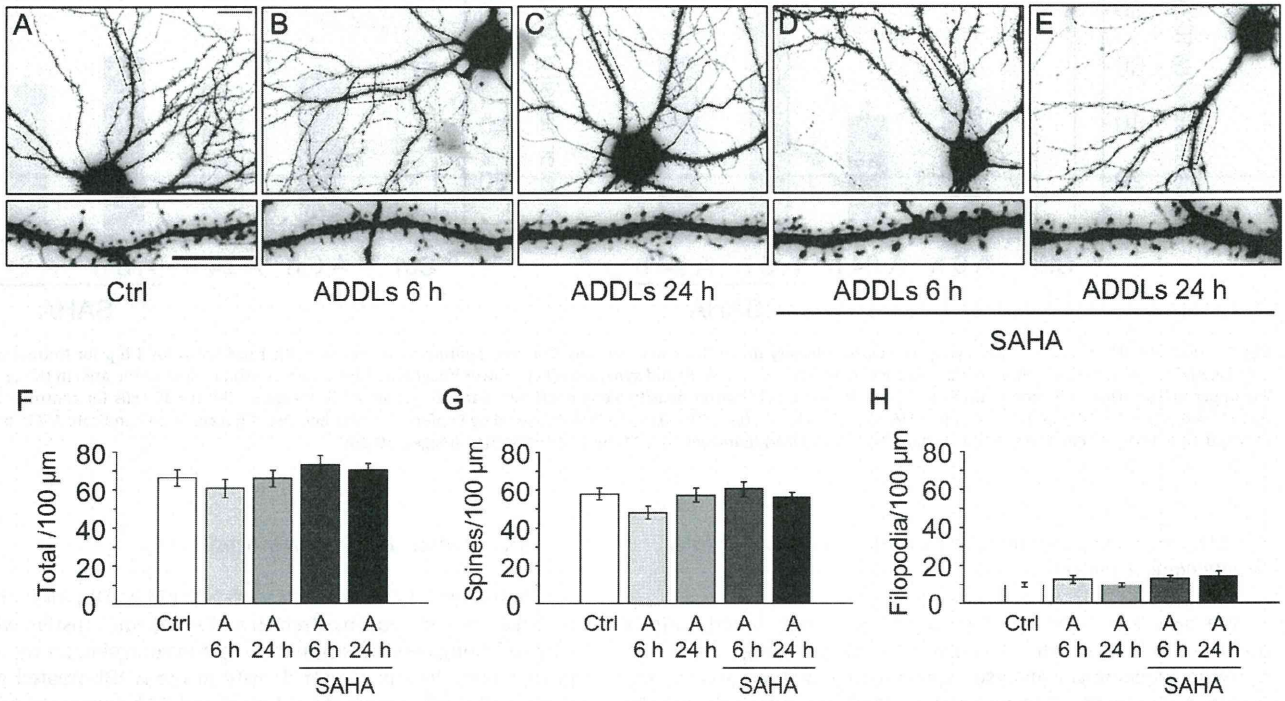

Fig. 7. Effect of ADDLs on protrusion density along dendrites. GFP-transfected neurons (21 DIV) were treated with 1 μM SAHA for 1 h prior to treatment with 100 nM ADDLs for 6 and 24 h. (A–E) GFP-fluorescence images of neurons. Lower images are high magnification images of the area in the rectangle in the upper images. (F–H) quantification of the density of total protrusions (spines and filopodia), spines, and filopodia along dendrites. A 6 and A 24 h represent ADDL treatments of 6 and 24 h, respectively. Data are presented as means ± SEM, $n = 28$, 28, 29, 27 and 33 cells for control, ADDLs 6 h, ADDLs 24 h, SAHA + ADDLs 6 h and SAHA + ADDLs 24 h, respectively; total protrusion density, $P = 0.295$; spine density, $P = 0.145$; filopodium density, $P = 0.105$, ANOVA. Scale bars: low magnification images, 20 μM; high magnification images, 10 μm.

4. Discussion

The present study demonstrates that acute SAHA treatment for 24 h attenuates ADDL-induced drebrin loss from dendritic spines. It was reported that chronic SAHA treatment for 10 days increases spine density (Guan et al., 2009). However, the relatively short 24-h period of SAHA treatment did not increase protrusion density in this study. This suggests that the protective effect of acute SAHA treatment on neurons exposed to ADDLs is not due to an increase in spine density.

Histone acetylation positively regulates the expression of various proteins that play important roles in synaptic function (Gräff and Tsai, 2013). Therefore, SAHA may induce the expression of some synaptic proteins by increasing levels of histone acetylation. Accordingly, we can infer that the ability of SAHA to protect against ADDL-induced drebrin loss may be associated with enhanced expression of synaptic proteins involved in the stabilization of the actin cytoskeleton in dendritic spines.

It is known that activation of NMDA receptors results in a decrease in drebrin in dendritic spines (Sekino et al., 2006). Because ADDLs induce the abnormal activation of NMDA receptors (De Felice et al., 2007; Lacor et al., 2007), the ADDL-induced decrease in drebrin cluster density may be mediated by abnormal activation of NMDA receptors. We recently showed that the activation of myosin II ATPase by Ca^{2+} influx through NMDA receptors induces the translocation of drebrin A from dendritic spines (Mizui et al., 2014). Therefore, SAHA may induce the expression of a protein that inhibits Ca^{2+} signal transduction, such as a factor that reduces or blocks binding of a Ca^{2+} sensor to Ca^{2+}, resulting in the inactivation of myosin II ATPase. This inactivation of myosin II ATPase may underlie the inhibition of drebrin loss from dendrites in neurons treated with SAHA. Alternatively, SAHA might inhibit myosin II ATPase by inactivating myosin light chain kinase (MLCK), because MLCK can enhance myosin II ATPase activity by phosphorylating the light chain of the protein. However, this is an unlikely possibility, because it has been reported that MLCK is not involved in the drebrin exodus from dendritic spines induced by NMDA receptor activation (Mizui et al., 2014). SAHA could also possibly suppress ADDL-induced drebrin loss from dendritic spines by inhibiting NMDA receptors. However, the present study shows that SAHA treatment does not change drebrin cluster density in control neurons. Thus, this possibility is also unlikely because the inhibition of NMDA receptors increases the accumulation of drebrin at dendritic spines (Mizui et al., 2014). Consequently, we consider it more likely that, by inhibiting HDAC, SAHA attenuates Ca^{2+} signaling by inducing gene expression in ADDL-treated neurons.

Following the drebrin exodus from dendritic spines, re-entry of the protein into these structures occurs during long-term potentiation (Mizui et al., 2014). Thus, ADDLs might inhibit re-entry of drebrin into dendritic spines, resulting in drebrin loss from these structures. By inhibiting HDAC, SAHA may induce the expression of a protein that promotes the re-entry of drebrin into dendritic spines. Therefore, HDAC might suppress the expression of a protein involved in the re-entry of drebrin into dendritic spines after ADDL exposure.

It was reported that ADDLs induce neuronal cell death *in vitro* (Chong et al., 2006; Geng et al., 2013). In the present study, however, ADDL-induced drebrin loss from dendritic spines was not non-specific protein degradation in the process of cell death, because the density of dendritic protrusions and synapsin I clusters was not decreased. This suggests that ADDL-induced drebrin loss from dendritic spines is due to a change in distribution of drebrin, similar to the drebrin exodus induced by NMDA receptor activation (Sekino et al., 2006; Mizui et al., 2014). Because micromolar levels of ADDLs were used in the cell-death study, the 100-nM concentration of ADDLs used in this study is likely insufficient to induce neuronal cell death.

It has been reported that drebrin expression is decreased in AD brains (Harigaya et al., 1996; Counts et al., 2012). In the present study, however, 100 nM ADDLs did not reduce the expression of drebrin, although the cluster density was reduced. In comparison, a high-dose of ADDLs (500 nM) reduced drebrin expression. Therefore, it is possible that drebrin loss from dendritic spines occurs prior to the reduction in drebrin expression in the progression of AD. ADDL-induced drebrin loss from dendritic spines might occur at the prodromal stage of AD. Therefore, HDAC inhibition might suppress clinical symptoms in this early stage of AD by attenuating the toxic effects of ADDLs on dendritic spine architecture. Similarly, ADDL-induced drebrin loss from dendritic spines may occur in depression, because Aβ levels are increased in the brains of patients with depression. Therefore, HDAC inhibitors might also hold therapeutic potential in patients with depression.

5. Conclusion

We demonstrate that ADDLs induce drebrin loss from dendritic spines in cultured hippocampal neurons without reducing drebrin expression or dendritic protrusion density. In addition, the inhibition of HDAC by SAHA attenuated ADDL-induced drebrin loss from dendritic spines. These results strongly suggest that the regulation of histone acetylation/deacetylation plays an important role in modulating actin cytoskeletal dynamics by inducing gene expression under cellular stress. Our findings provide insight into the mechanisms of amyloid toxicity and suggest that HDAC inhibitors may hold therapeutic potential in neuropsychiatric disorders, such as AD and depression.

Acknowledgments

We would like to thank Dr. Hiroyuki Yamazaki for useful discussions in this study. A part of this study is the result of "Integrated Research on Neuropsychiatric Disorders" carried out under the Strategic Research Program for Brain Sciences by the Ministry of Education, Culture, Sports, Science and Technology of Japan, and JSPS Grant-in-Aid for Young Scientists (B) Grant Number 26830042. All of the authors declare no conflict of interest regarding the manuscript.

References

Chong, Y.H., Shin, Y.J., Lee, E.O., Kayed, R., Glabe, C.G., Tenner, A.J., 2006. ERK1/2 activation mediates Abeta oligomer-induced neurotoxicity via caspase-3 activation and tau cleavage in rat organotypic hippocampal slice cultures. J. Biol. Chem. 281, 20315–20325.

Counts, S.E., He, B., Nadeem, M., Wuu, J., Scheff, S.W., Mufson, E.J., 2012. Hippocampal drebrin loss in mild cognitive impairment. Neurodegener. Dis. 10, 216–219.

De Felice, F.G., Velasco, P.T., Lambert, M.P., Viola, K., Fernandez, S.J., Ferreira, S.T., Klein, W.L., 2007. Abeta oligomers induce neuronal oxidative stress through an N-methyl-D-aspartate receptor-dependent mechanism that is blocked by the Alzheimer drug memantine. J. Biol. Chem. 282, 11590–11601.

Fa, M., Orozco, I.J., Francis, Y.I., Saeed, F., Gong, Y., Arancio, O., 2010. Preparation of oligomeric beta-amyloid 1-42 and induction of synaptic plasticity impairment on hippocampal slices. J. Vis. Exp.

Flavell, S.W., Greenberg, M.E., 2008. Signaling mechanisms linking neuronal activity to gene expression and plasticity of the nervous system. Annu. Rev. Neurosci. 31, 563–590.

Francis, Y.I., Fà, M., Ashraf, H., Zhang, H., Staniszewski, A., Latchman, D.S., Arancio, O., 2009. Dysregulation of histone acetylation in the APP/PS1 mouse model of Alzheimer's disease. J. Alzheimers Dis. 18, 131–139.

Geng, D., Kang, L., Su, Y., Jia, J., Ma, J., Li, S., Du, J., Cui, H., 2013. Protective effects of EphB2 on Aβ1-42 oligomer-induced neurotoxicity and synaptic NMDA receptor signaling in hippocampal neurons. Neurochem. Int. 63, 283–290.

Goldberg, A.D., Allis, C.D., Bernstein, E., 2007. Epigenetics: a landscape takes shape. Cell 128, 635–638.

Gräff, J., Tsai, L.H., 2013. Histone acetylation: molecular mnemonics on the chromatin. Nat. Rev. Neurosci. 14, 97–111.

Guan, J.S., Haggarty, S.J., Giacometti, E., Dannenberg, J.H., Joseph, N., Gao, J., Nieland, T.J., Zhou, Y., Wang, X., Mazitschek, R., Bradner, J.E., DePinho, R.A., Jaenisch, R., Tsai, L.H., 2009. HDAC2 negatively regulates memory formation and synaptic plasticity. Nature 459, 55–60.

Harigaya, Y., Shoji, M., Shirao, T., Hirai, S., 1996. Disappearance of actin-binding protein, drebrin, from hippocampal synapses in Alzheimer's disease. J. Neurosci. Res. 43, 87–92.

Hayashi, K., Shirao, T., 1999. Change in the shape of dendritic spines caused by overexpression of drebrin in cultured cortical neurons. J. Neurosci. 19, 3918–3925.

Ishizuka, Y., Kakiya, N., Witters, L.A., Oshiro, N., Shirao, T., Nawa, H., Takei, N., 2013. AMP-activated protein kinase counteracts brain-derived neurotrophic factor-induced mammalian target of rapamycin complex 1 signaling in neurons. J. Neurochem. 127, 66–77.

Kilgore, M., Miller, C.A., Fass, D.M., Hennig, K.M., Haggarty, S.J., Sweatt, J.D., Rumbaugh, G., 2010. Inhibitors of class 1 histone deacetylases reverse contextual memory deficits in a mouse model of Alzheimer's disease. Neuropsychopharmacology 35, 870–880.

Knafo, S., Alonso-Nanclares, L., Gonzalez-Soriano, J., Merino-Serrais, P., Fernaud-Espinosa, I., Ferrer, I., DeFelipe, J., 2009. Widespread changes in dendritic spines in a model of Alzheimer's disease. Cereb. Cortex 19, 586–592.

Kumar, A., Kepe, V., Barrio, J.R., Siddarth, P., Manoukian, V., Elderkin-Thompson, V., Small, G.W., 2011. Protein binding in patients with late-life depression. Arch. Gen. Psychiatry 68, 1143–1150.

Kurdistani, S.K., Grunstein, M., 2003. Histone acetylation and deacetylation in yeast. Nat. Rev. Mol. Cell Biol. 4, 276–284.

Lacor, P.N., Buniel, M.C., Furlow, P.W., Clemente, A.S., Velasco, P.T., Wood, M., Viola, K.L., Klein, W.L., 2007. Abeta oligomer-induced aberrations in synapse composition, shape, and density provide a molecular basis for loss of connectivity in Alzheimer's disease. J. Neurosci. 27, 796–807.

Lambert, M.P., Viola, K.L., Chromy, B.A., Chang, L., Morgan, T.E., Yu, J., Venton, D.L., Krafft, G.A., Finch, C.E., Klein, W.L., 2001. Vaccination with soluble Abeta oligomers generates toxicity-neutralizing antibodies. J. Neurochem. 79, 595–605.

Lee, D., Aoki, C., 2012. Presenilin conditional double knockout mice exhibit decreases in drebrin a at hippocampal CA1 synapses. Synapse 66, 870–879.

Lue, L.F., Kuo, Y.M., Roher, A.E., Brachova, L., Shen, Y., Sue, L., Beach, T., Kurth, J.H., Rydel, R.E., Rogers, J., 1999. Soluble amyloid beta peptide concentration as a predictor of synaptic change in Alzheimer's disease. Am. J. Pathol. 155, 853–862.

Mizui, T., Sekino, Y., Yamazaki, H., Ishizuka, Y., Takahashi, H., Kojima, N., Kojima, M., Shirao, T., 2014. Myosin II ATPase activity mediates the long-term potentiation-induced exodus of stable F-actin bound by drebrin a from dendritic spines. PLoS One 9, e85367.

Sekino, Y., Tanaka, S., Hanamura, K., Yamazaki, H., Sasagawa, Y., Xue, Y., Hayashi, K., Shirao, T., 2006. Activation of N-methyl-D-aspartate receptor induces a shift of drebrin distribution: disappearance from dendritic spines and appearance in dendritic shafts. Mol. Cell. Neurosci. 31, 493–504.

Shankar, G.M., Bloodgood, B.L., Townsend, M., Walsh, D.M., Selkoe, D.J., Sabatini, B.L., 2007. Natural oligomers of the Alzheimer amyloid-beta protein induce reversible synapse loss by modulating an NMDA-type glutamate receptor-dependent signaling pathway. J. Neurosci. 27, 2866–2875.

Shirao, T., Obata, K., 1985. Two acidic proteins associated with brain development in chick embryo. J. Neurochem. 44, 1210–1216.

Shirao, T., González-Billault, C., 2013. Actin filaments and microtubules in dendritic spines. J. Neurochem. 126, 155–164.

Takahashi, H., Sekino, Y., Tanaka, S., Mizui, T., Kishi, S., Shirao, T., 2003. Drebrin-dependent actin clustering in dendritic filopodia governs synaptic targeting of postsynaptic density-95 and dendritic spine morphogenesis. J. Neurosci. 23, 6586–6595.

Uchida, H., Ma, L., Ueda, H., 2010. Epigenetic gene silencing underlies C-fiber dysfunctions in neuropathic pain. J. Neurosci. 30, 4806–4814.

Yamazaki, H., Kojima, N., Kato, K., Hirose, E., Iwasaki, T., Mizui, T., Takahashi, H., Hanamura, K., Roppongi, R.T., Koibuchi, N., Sekino, Y., Mori, N., Shirao, T., 2014. Spikar, a novel drebrin-binding protein, regulates the formation and stabilization of dendritic spines. J. Neurochem. 128, 507–522.

Zhao, L., Ma, Q.L., Calon, F., Harris-White, M.E., Yang, F., Lim, G.P., Morihara, T., Ubeda, O.J., Ambegaokar, S., Hansen, J.E., Weisbart, R.H., Teter, B., Frautschy, S.A., Cole, G.M., 2006. Role of p21-activated kinase pathway defects in the cognitive deficits of Alzheimer disease. Nat. Neurosci. 9, 234–242.

Comparison of the radiosensitivities of neurons and glial cells derived from the same rat brain

SHIGEHIRO KUDO[1], YOSHIYUKI SUZUKI[1], SHIN-EI NODA[1], TOSHIYUKI MIZUI[2], KATSUYUKI SHIRAI[1], MASAHIKO OKAMOTO[1], TAKUYA KAMINUMA[1], YUKARI YOSHIDA[3], TOMOAKI SHIRAO[2] and TAKASHI NAKANO[1]

Departments of [1]Radiation Oncology and [2]Neurobiology and Behavior, Gunma University Graduate School of Medicine; [3]Gunma University Heavy Ion Medical Center, Maebashi, Gunma 371-8511, Japan

Received February 5, 2014; Accepted June 13, 2014

DOI: 10.3892/etm.2014.1802

Abstract. Non-proliferating cells, such as mature neurons, are generally believed to be more resistant to X-rays than proliferating cells, such as glial and vascular endothelial cells. Therefore, the late adverse effects of radiotherapy on the brain have been attributed to the radiation-induced damage of glial and vascular endothelial cells. However, little is known about the radiosensitivities of neurons and glial cells due to difficulties in culturing these cells, particularly neurons, independently. In the present study, primary dissociated neurons and glial cultures were prepared separately from the hippocampi and cerebrum, respectively, which had been obtained from the same fetal rat on embryonic day 18. X-irradiations of 50 Gy were performed on the cultured neurons and glial cells at 7 and 21 days *in vitro* (DIV). The cells were fixed at 24 h after irradiation. Terminal deoxynucleotidyl transferase-mediated dUTP nick end labeling was then performed to measure the apoptotic indices (AIs). The AIs of non-irradiated and irradiated neurons at 7 DIV were 23.7±6.7 and 64.9±4.8%, and those at 21 DIV were 52.1±17.4 and 44.6±12.5%, respectively. The AIs of non-irradiated and irradiated glial cells at 7 DIV were 5.8±1.5 and 78.4±3.3% and those at 21 DIV were 9.6±2.6 and 86.3±4.9%, respectively. Glial cells and neurons were radiosensitive at 7 DIV. However, while glial cells were radiosensitive at 21 DIV, neurons were not.

Introduction

Radiation therapy is among the essential treatment modalities for primary and metastatic brain tumors. However, subsequent cognitive function decline and developmental disorders following radiation therapy to the brain must be overcome, particularly in pediatric patients (1-5).

The central nervous system (CNS) is composed mainly of neurons, glial cells and vascular endothelial cells (Fig. 1). Neurons, the majority of which cease cell proliferation during fetal development, have been considered to be more radioresistant than glial and vascular endothelial cells, which continue to proliferate subsequent to birth. Molecular studies have provided evidence that glial cells are essential for the survival of neurons by supplying trophic factors to the neurons (6-9). Thus, the mechanism underlying the late adverse brain effects of radiation therapy has been believed to mainly be the insufficient supply of nutrients and blood to neurons due to the impaired functions of irradiated glial and vascular endothelial cells, rather than a direct effect of the radiation itself on neurons.

It was shown in the late 1990s that adult neurogenesis occurs in certain areas of the brain, including the subventricular zone (SVZ) and subgranular layer (SGL) (10). In addition, radiation-induced apoptosis of neural progenitor cells was observed in the SVZ and SGL, and relatively high radiosensitivity was demonstrated in neurons residing in the areas where neurogenesis occurs (11,12). These findings have raised the possibility that radiation-induced neuronal death may be one of the causes of the late adverse effects of radiation therapy, such as functional and developmental disorders. Therefore, attempts have been made to prevent adverse effects from developing following cranial irradiation using intensity-modulated radiation therapy to reduce the dose to areas that may be highly radiosensitive, such as the SVZ and SGL (13-16).

Radiation affects neurons and glial and vascular endothelial cells. It is therefore difficult to evaluate the radiation sensitivities of these cell types separately in *in vivo* studies. Furthermore, the majority of the previously reported *in vitro* studies were conducted on a mixture of neurons and glial cells (17). However, due to technical difficulties, only a few investigations, including our previous studies (18,19), have examined the radiosensitivity of neurons by employing monocultures of this cell type alone.

To estimate the extent of the involvement of neurons and glial cells in the adverse brain effects of radiation therapy, it

Correspondence to: Dr Yoshiyuki Suzuki, Department of Radiation Oncology, Gunma University Graduate School of Medicine, 3-39-22, Showa-machi, Maebashi, Gunma 371-8511, Japan
E-mail: syoshi@gunma-u.ac.jp

Key words: neuron, glia, radiation, apoptosis

is essential to compare radiosensitivities between glial cells and neurons. A previous study using glial cells and neurons cultured separately for such a comparison demonstrated the radiosensitivity of glial cells to be comparable to that of neurons (17). However, the cells used in that study were isolated from different individuals (different genetic backgrounds) and cultured for different lengths of time (different developmental stages), such that the results are not entirely convincing. In the present study, neurons and glial cells were therefore obtained from the same rat to ensure uniform conditions (identical genetic backgrounds and developmental stages) and their radiosensitivities were investigated separately.

Materials and methods

Cell culture. The modified Banker's method was used for primary neuronal cultures (20). Briefly, cells were obtained from the hippocampi of Wistar rat fetuses (Imai Jikkendobutu Shiikujo, Saitama, Japan) at embryonic day 18, treated with trypsin and mechanically dispersed by trituration with Pasteur pipettes. The cells were then seeded at a density of 5,000 cells/cm^2 on glass coverslips coated with poly-L-lysine and cultured in minimum essential medium (MEM; Invitrogen Life Technologies, San Diego, CA, USA) for 3 h. The coverslips were then transferred to culture dishes containing a monolayer of supporting glial cells maintained in serum-free MEM supplemented with B27 (Invitrogen Life Technologies). Cytosine β-D-arabinofuranoside (Sigma, St. Louis, MO, USA) (10 μM) was added to the culture medium at 3 days *in vitro* (DIV) to inhibit glial cell proliferation. Neurons were irradiated at 7 or 21 DIV. For X-irradiation of the cells, the cover slips were transferred to another culture dish containing only medium and no glial cells. Immediately subsequent to the irradiation of the neurons, the cover slips were returned to the original culture dishes. Although the neurons were in direct contact with the glial cells, they were easily separable; thus, it was possible to irradiate and observe only neurons.

Glial cells were obtained from the cerebral cortex of the same Wistar rat fetus as that used for obtaining neurons at embryonic day 18. Briefly, the cells were treated with trypsin, dispersed by trituration with Pasteur pipettes and then seeded at a density of 5,000 cell/cm^2 on glass coverslips coated with poly-L-lysine and cultured in MEM. Four days later, the cells were again treated with trypsin, dispersed with Pasteur pipettes and then cultured in new MEM. Glial cells were also irradiated at 7 DIV or 21 DIV. For X-irradiation of the cells, the cover slips were transferred to another culture dish containing only medium and no glial cells. Following irradiation of the glial cells, the cover slips were returned to the original culture dishes.

All animal experiments were performed in accordance with the guidelines set by the Animal Care and Experimentation Committee (Gunma University, Maebashi, Japan).

Irradiation and cell fixation. At 7 and 21 DIV, neural and glial cells were irradiated with 200 kV X-rays (Siemens-Asahi Medical Technologies Ltd., Tokyo, Japan) at a dose of 50 Gy. At 24 h after irradiation, the cells were fixed in 4% paraformaldehyde for 24 h at 4˚C. Non-irradiated culture cells were handled in parallel with the irradiated samples as a control.

Assessment of apoptosis. Apoptosis was determined by terminal deoxynucleotidyl transferase-mediated dUTP nick end labeling (TUNEL) assay using the ApopTag® Plus *In Situ* Apoptosis Fluorescein Detection kit (Chemicon International, Temecula, CA, USA). Fixed cells on coverslips were permeabilized in ethanol:acetic acid (2:1) for 15 min at -20˚C. The cells were then washed twice with phosphate-buffered saline (pH 7.4) for 5 min and incubated with ApopTag equilibration buffer for 5 min, followed by terminal deoxynucleotidyl transferase linkage of digoxigenin-tagged dUTP to the 3'-OH termini of DNA fragments at 37˚C for 60 min. The reaction was terminated at 37˚C in stop/wash buffer for 30 min and the cells were then washed. Subsequent to washing, the cells were incubated with anti-digoxigenin fluorescein antibody for 30 min and the coverslips were then mounted on slides with Vectashield® Mounting Medium with DAPI (Vector Laboratories, Burlingame, CA, USA).

Evaluation method. Fluorescein-labeled cells were observed under a Zeiss Axioplan microscope (Carl Zeiss AG, Jena, Germany) equipped with a Photometrics CoolSnap FX cooled CCD camera (Photometrics, Tucson, AZ, USA) using MetaMorph software (Universal Imaging Corp., West Chester, PA, USA). Apoptotic cells were counted on each slide. The apoptotic index (AI) was calculated as the number of DAPI- and TUNEL-positive cells divided by the number of DAPI-positive cells. The cells positive for TUNEL and negative for DAPI were excluded from the calculations.

Statistical analysis. Statistical analysis was performed using StatMate software (GraphPad Software, Inc., San Diego, CA, USA). $P<0.01$, as determined using a Student's t-test, was considered to indicate a statistically significant difference. All results are shown as the mean ± standard deviation.

Results

The average numbers of neurons and glial cells counted in each coverslip were 332 (range, 211-556) and 273 (range, 131-292), respectively. Representative images of irradiated neurons are shown in Fig. 2. The AI of 7 DIV neurons was 23.7±6.7% (n=3) in the control group and significantly higher, 64.9±4.8% (n=3), in the 50 Gy irradiated group ($P<0.001$) (Fig. 3A). At 21 DIV, the AI of neurons was 52.1±17.4% (n=9) in the control group and 44.6±12.5% (n=8) in the irradiated group; no significant difference was identified in the number of apoptotic cells between the two groups ($P=0.61$) (Fig. 3B). The average AI of 7 DIV glial cells was 5.8±1.5% (n=3) in the control group and 78.4±3.3% (n=3) in the 50 Gy irradiated group (Fig. 3C), and the average AI of 21 DIV glial cells was 9.6±2.6% (n=4) in the control group and 86.3±4.9% (n=4) in the 50 Gy irradiated group (Fig. 3D). The differences between the control and 50 Gy irradiated groups were significant at 7 DIV ($P<0.001$) as well as at 21 DIV ($P<0.001$).

Comparisons at the corresponding time-points revealed both glial cells and neurons to be radiosensitive at 7 DIV,

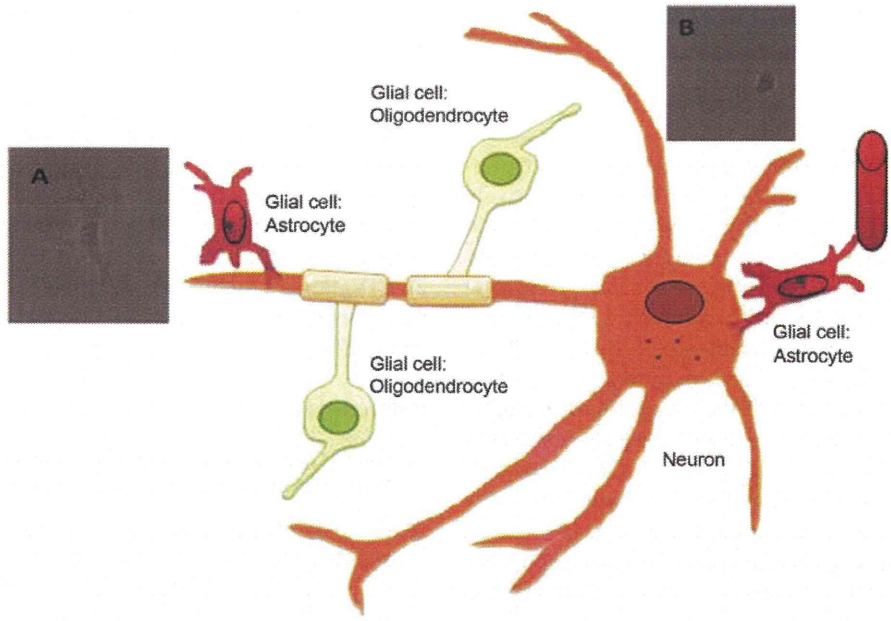

Figure 1. Illustration depicting the associations between neurons and glial cells in the CNS. The CNS is composed mainly of neurons and glial cells (astrocytes, oligodendrocytes and microglia). Glial cells are essential for the survival of neurons as they supply trophic factors to the neurons. (A and B) Phase contrast images show a (A) glial cell and (B) neuron. CNS, central nervous system. Magnification, x20.

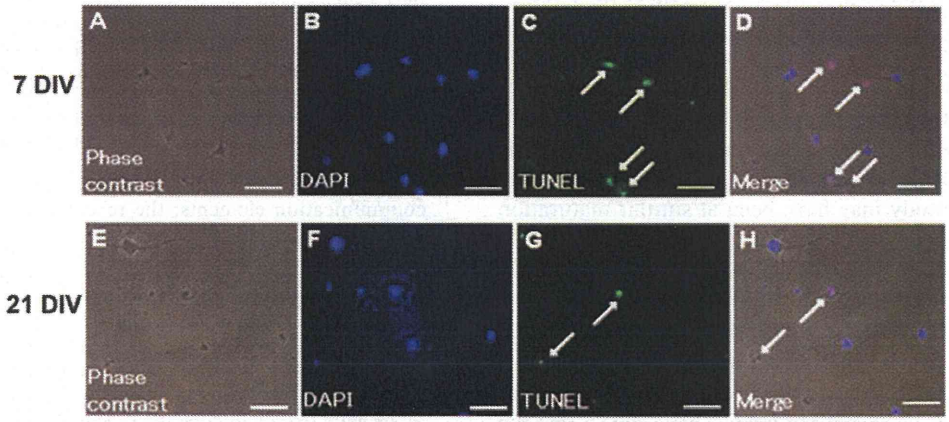

Figure 2. TUNEL analysis of cells undergoing radiation-induced apoptosis. (A-D) 7 DIV neurons; (E-H) 21 DIV neurons. (A and E) Phase contrast images; (B and F) DAPI fluorescence images; (C and G) TUNEL fluorescence images; (D and H) double fluorescence images for TUNEL (red) and DAPI (blue). Scale bar = 50 μm. DIV, days *in vitro*; TUNEL, terminal deoxynucleotidyl transferase-mediated dUTP nick end labeling. Magnification, x20. The arrows indicate nuclear pylnosis.

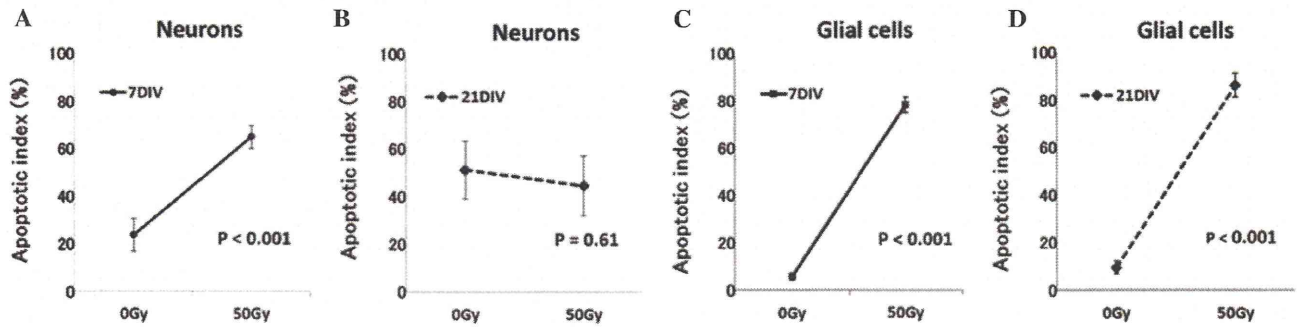

Figure 3. Plots of the average AIs of cells irradiated with 0 Gy (Control) or 50 Gy, at 7 or 21 DIV. Neurons: (A) The AI was significantly increased by 50 Gy irradiation at 7 DIV as compared with the control (n=3, P<0.001). (B) No increase in AI was identified at 21 DIV (n=8, P=0.61). Glial cells: The AI increased significantly with 50 Gy irradiation at both (C) 7 DIV and (D) 21 DIV (7 DIV, n=3, P<0.001; 21 DIV, n=4, P<0.001). The bars represent standard deviations. DIV, days *in vitro*; AI, apoptotic index.

whereas glial cells but not neurons were radiosensitive at 21 DIV.

Discussion

Our previous study revealed 7 DIV neurons (morphologically and functionally immature cells) to be relatively radiosensitive, while 21 DIV neurons (morphologically and functionally mature cells) were found to be extremely radioresistant, showing no increase in apoptosis even following high-dose irradiation (19). Furthermore, when 7 DIV neurons were exposed to low doses of X-irradiation (0, 5, 4 and 10 Gy) and further cultured for 14 and 21 days in total, the number of apoptotic cells increased, and the clustering of synaptic proteins, indicative of the maturation of synapses, decreased dose-dependently following irradiation (18). Consistent with our previous findings, the present results showed that the number of 7 DIV neurons undergoing apoptosis increased following irradiation, whereas radiation did not significantly increase apoptosis in 21 DIV neurons. These results indicate that radiosensitive immature neurons become radioresistant with maturation and that mature neurons are radioresistant.

The AI of glial cells did not differ significantly between 7 and 21 DIV in this study. Although no study has focused on the association between the maturity and radiosensitivity of glial cells, if the maturities of these cells reflect their radiosensitivity, our present results may suggest their maturities to be similar at 7 and 21 DIV. In other words, since glial cells have the ability to proliferate (gliogenesis), unlike neurons, it is assumed that a glial cell population would represent a mixture of cells with differing maturities due to this proliferation. Thus, their similar radiosensitivities suggest that the glial cells in this study may have been at similar maturation stages.

Following irradiation, glial cells may undergo mitotic cell death. Furthermore, we observed in a previous study that a large percentage of neurons underwent delayed apoptosis subsequent to irradiation (18). Thus, comparing the radiosensitivities of neurons and glial cells based on their AIs at 24 h after irradiation can be difficult. A number of studies have shown that the ability to repair radiation damage differs among sites (10,21). Eriksson *et al* (10) reported that adult neurogenesis occurs in both the SVZ and the SGL, and Seaberg *et al* (21) showed that stem cells with pluripotency and self-renewal ability were present in the SVZ, while the SGL contained predominantly neural progenitor cells without pluripotency and fewer stem cells. In other words, due to the presence of radioresistant and pluripotent stem cells in the SVZ, neurogenesis may occur following irradiation in this area, whereas recovery subsequent to irradiation may be poor in the SGL where the number of the stem cells is limited. In a study by Hellström *et al* (22), the volume and rate of DNA synthesis following whole brain irradiation were reported to be significantly higher in the SVZ than in the SGL (22). Glial cells have the ability to proliferate, such that damaged glial cells can be replaced by gliogenesis. Therefore, to understand the mechanisms underlying the adverse effects of radiation therapy on the brain, the neurogenesis, restoration of glial cells and secondary effects due to brain blood vessels being impaired by irradiation must all be taken into consideration. Furthermore, radiation effects on the brain may vary according to the irradiation site, extent and dose, due to the heterogeneous distribution of neural stem cells.

In conclusion, the radiosensitivities of neurons and glial cells, obtained from the same rat brain, were evaluated by examining the number of cells undergoing radiation-induced apoptosis. The results showed both glial cells and neurons to be radiosensitive at 7 DIV, whereas only glial cells were radiosensitive at 21 DIV; neurons exhibited radioresistance at 21 DIV. Further studies are required to elucidate the mechanisms underlying the late adverse effects of radiation therapy on the CNS.

References

1. Hall EJ and Giaccia AJ (eds): Radiobiology for the Radiologist. Sixth edition. Lippincott Williams & Wilkins, Philadelphia, PA, 2006.
2. Chang EL, Wefel JS, Hess KR, *et al*: Neurocognition in patients with brain metastases treated with radiosurgery or radiosurgery plus whole-brain irradiation: a randomised controlled trial. Lancet Oncol 10: 1037-1044, 2009.
3. Nakaya K, Hasegawa T, Flickinger JC, Kondziolka DS, Fellows-Mayle W and Gobbel GT: Sensitivity to radiation-induced apoptosis and neuron loss declines rapidly in the postnatal mouse neocortex. Int J Radiat Biol 81: 545-554, 2005.
4. Shi L, Molina DP, Robbins ME, Wheeler KT and Brunso-Bechtold JK: Hippocampal neuron number is unchanged 1 year after fractionated whole-brain irradiation at middle age. Int J Radiat Oncol Biol Phys 71: 526-532, 2008.
5. Takadera T, Sakamoto Y and Ohyashiki T: NMDA receptor 2B-selective antagonist ifenprodil-induced apoptosis was prevented by glycogen synthase kinase-3 inhibitors in cultured rat cortical neurons. Brain Res 1020: 196-203, 2004.
6. Allen NJ and Barres BA: Signaling between glia and neurons: focus on synaptic plasticity. Curr Opin Neurobiol 15: 542-548, 2005.
7. Volterra A and Meldolesi J: Astrocytes, from brain glue to communication elements: the revolution continues. Nat Rev Neurosci 6: 626-640, 2005.
8. Yamazaki Y, Hozumi Y, Kaneko K, *et al*: Direct evidence for mutual interactions between perineuronal astrocytes and interneurons in the CA1 region of the rat hippocampus. Neuroscience 134: 791-802, 2005.
9. Ye ZC and Sontheimer H: Astrocytes protect neurons from neurotoxic injury by serum glutamate. Glia 22: 237-248, 1998.
10. Eriksson PS, Perfilieva E, Björk-Eriksson T, *et al*: Neurogenesis in the adult human hippocampus. Nat Med 4: 1313-1317, 1998.
11. Peissner W, Kocher M, Treuer H and Gillardon F: Ionizing radiation-induced apoptosis of proliferating stem cells in the dentate gyrus of the adult rat hippocampus. Brain Res Mol Brain Res 71: 61-68, 1999.
12. Tada E, Parent JM, Lowenstein DH and Fike JR: X-irradiation causes a prolonged reduction in cell proliferation in the dentate gyrus of adult rats. Neuroscience 99: 33-41, 2000.
13. Barani IJ, Cuttino LW, Benedict SH, *et al*: Neural stem cell-preserving external-beam radiotherapy of central nervous system malignancies. Int J Radiat Oncol Biol Phys 68: 978-985, 2007.
14. Ghia A, Tomé WA, Thomas S, *et al*: Distribution of brain metastases in relation to the hippocampus: implications for neurocognitive functional preservation. Int J Radiat Oncol Biol Phys 68: 971-977, 2007.
15. Gutiérrez AN, Westerly DC, Tomé WA, *et al*: Whole brain radiotherapy with hippocampal avoidance and simultaneously integrated brain metastases boost: a planning study. Int J Radiat Oncol Biol Phys 69: 589-597, 2007.
16. Jaganathan A, Tiwari M, Phansekar R, Panta R and Huilgol N: Intensity-modulated radiation to spare neural stem cells in brain tumors: a computational platform for evaluation of physical and biological dose metrics. J Cancer Res Ther 7: 58-63, 2011.
17. Gobbel GT, Bellinzona M, Vogt AR, Gupta N, Fike JR and Chan PH: Response of postmitotic neurons to X-irradiation: implications for the role of DNA damage in neuronal apoptosis. J Neurosci 18: 147-155, 1998.